# Heat Transfer Augmentation Downstream of Rows of Various Dimple Geometries on the Suction Side of a Gas Turbine Airfoil

**Jason E. Dees**

**David G. Bogard**

University of Texas,
1 University Station C 2200,
Austin, TX 78712

**Ronald S. Bunker**
GE Global Research,
One Research Circle,
Niskayuna, NY 12309

*Heat transfer coefficients were measured downstream of a row of shaped film cooling holes, as well as elliptical, diffuser, and teardrop shaped dimples, simulating depressions due to film coolant holes of different shapes. These features were placed on the suction side of a simulated gas turbine vane. The dimples were used as approximations to film cooling holes after the heat transfer levels downstream of active fan shaped film cooling holes was found to be independent of film cooling. The effects of the dimples were tested with varying approach boundary layers, freestream turbulence intensity, and Reynolds numbers. For the case of an untripped (transitional) approach boundary layer, all dimple shapes caused approximately a factor of 2 increase in heat transfer coefficient relative to the smooth baseline condition due to the dimples effectively causing boundary layer transition downstream. The exact augmentation varied depending on the dimple geometry: diffuser shapes causing the largest augmentation and teardrop shapes causing the lowest augmentation. For tripped (turbulent boundary layer) approach conditions, the dimple shapes all caused the same 20% augmentation relative to the smooth tripped baseline. The already turbulent nature of the tripped approach flow reduces the effect that the dimples have on the downstream heat transfer coefficient.* [DOI: 10.1115/1.3149284]

## 1 Introduction

Today's modern gas turbine engines are subjected to combustor exit temperatures that exceed the material melting temperatures. For this reason, engine components must be cooled. Film cooling employs the use of coolant holes machined into turbine components. Relatively cool compressor bleed air is ejected through the film cooling holes in an effort to shield the material surface from the hot mainstream gas. An unfortunate side effect of film cooling is increased convective heat transfer coefficients resulting from the surface imperfection and the mainstream to film cooling jet interaction. In order to achieve the desired result of lower heat flux into the vane, the positive effects of the film coverage must outweigh the negative effects caused by the increased convective heat transfer coefficient. The heat transfer to a film cooled component is given by

$$q'' = h_f(T_{aw} - T_w) \tag{1}$$

Film cooling performance is dependent on several flow and geometric parameters. Flow parameters that affect film cooling include the coolant to mainstream mass flux ratio, density ratio, velocity ratio, and freestream turbulence intensity. Geometric parameters that affect the film cooling performance include the hole diameter, shape, coolant ejection angle, surface roughness, and the hole pitch to diameter and length to diameter ratios.

Eriksen and Goldstein [1] measured the heat transfer coefficient downstream of a single row of streamwise inclined cylindrical holes on a flat plate. This study showed that for higher blowing ratios ($1 < M < 2$) peak laterally averaged $h_f/h_0$ values ranged from 1.05 to 1.25 immediately downstream of coolant injection, decreasing to unity with increasing $x/d$. For a blowing ratio of $M = 0.5$, a slight decrease was seen directly downstream of coolant injection increasing to unity as $x/d$ increased. Similar studies [2–4] showed levels of laterally averaged $h_f/h_0$ immediately downstream of injection of 1.25–1.60, with higher augmentation levels generally corresponding to higher blowing ratios. In all of these studies, the $h_0$ reference condition was that of a fully turbulent boundary layer with an unheated starting length (UHSL).

The vast majority of film cooling heat transfer coefficient studies have examined the cylindrical film cooling hole, but a few studies have examined the effects of different hole shapes on the downstream heat transfer coefficient. Sargison et al. [5] measured heat transfer coefficients downstream of cylindrical and fan shaped cooling holes, a slot, and a "console" film cooling geometry. The results of this study were presented in terms of dimensional $h_f$ values. The shaped holes were found to have the same downstream laterally averaged heat transfer coefficient as the cylindrical holes for a momentum flux ratio of 1.1. The slot and console configurations both had downstream heat transfer coefficient values that were about 15% higher than the cylindrical and fan shaped holes and equal to the $h$ value predicted for a flat plate at the flow conditions. Interestingly, this suggests that for the flow conditions in this study, the film cooling from the discrete hole geometries would actually decrease the heat transfer coefficient.

Lu et al. [6] also measured the heat transfer coefficient augmentation downstream of a row of fan shaped film cooling holes with blowing ratios ranging $M = 0.5–2.0$. Laterally averaged $h_f/h_0$ values were presented for a fan shaped hole configuration, a cylindrical hole configuration, and several transverse trench configurations. The $h_0$ condition used in this case was the measured value for a fully turbulent boundary layer. The results of this study showed that the fan shaped holes caused 50–100% larger heat transfer augmentation values than the cylindrical holes and trench

Contributed by the International Gas Turbine Institute of ASME for publication in the JOURNAL OF TURBOMACHINERY. Manuscript received October 8, 2008; final manuscript received November 18, 2008; published online March 25, 2010. Review conducted by David Wisler. Paper presented at the ASME Turbo Expo 2008: Land, Sea and Air (GT2008), Berlin, Germany, June 9–13, 2008.

  

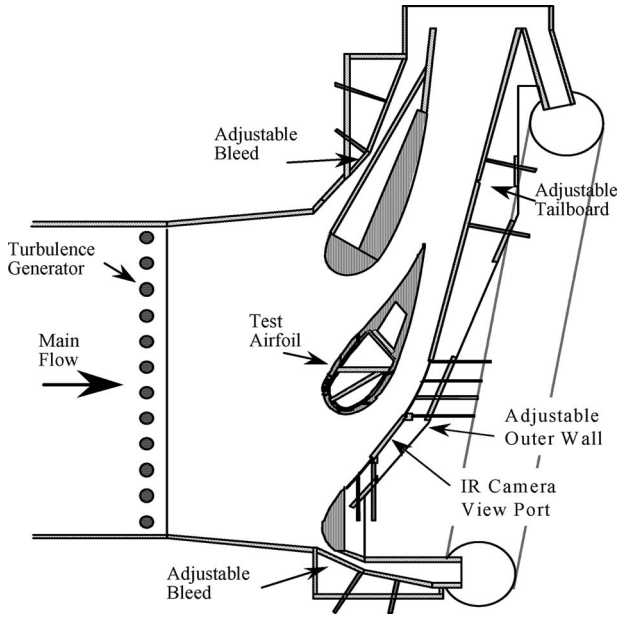


**Fig. 1 Schematic of the simulated turbine vane test section**

configurations for $M=0.5$ and $M=1.0$. As the blowing ratio increased beyond $M=1.0$, the shaped holes and trench configurations cause the same heat transfer augmentation, which is higher than the cylindrical holes case. Dittmar et al. [7] performed heat transfer coefficient measurements downstream of double rows of cylindrical hole and discrete slots, a single row of fan shaped holes, and a single row of compound angle fan shaped holes on a simulated vane suction side. The results of this study show that the fan shaped configurations all show $h_f/h_0=1.4-1.6$ immediately downstream of the holes, decreasing to a value of $h_f/h_0=1.1$ as the downstream distance increases to $x/d>30$.

The study presented in this paper examines the heat transfer augmentation downstream of a row of diffuser shaped film cooling holes with both heated starting length (HSL) and unheated starting length cases. Various dimple geometries designed to simulate different film cooling hole shapes were also included in the study. The dimple geometries were assumed to be good simulations of the active film holes due to the fact that film cooling at all blowing ratios, including $M=0$, was found to have no effect on the heat transfer coefficient downstream of the shaped holes. The dimples were a simple way to test several different simulated film cooling hole shapes.

## 2 Experimental Facilities and Procedures

Experiments were conducted in a closed loop wind tunnel driven by a 50 hp adjustable speed blower. The test section, shown in Fig. 1, simulated a three vane, two passage cascade. The vane geometry was taken from an actual turbine inlet guide vane scaled up nine times. For this study, only the suction side of the test vane was examined. Adjustable bypass flows outside of the two half vanes were designed to match the passage flow of three vanes. The outer wall of the test section had movable walls in order to control the pressure distribution around the test vane. The chord length of the scaled up test vane was 59.4 cm and the span was 54.9 cm. The vane cascade had a pitch of 45.7 cm. For the experiments performed in this study, the mainstream approach flow was held at 5.8 m/s for the low Reynolds number condition and at 10.5 m/s for the high Reynolds number condition. Previous measurements [8] showed the mainstream turbulence was $Tu=5.2\%$ and 21% at $0.18C$ upstream of the vane's leading edge for the low and high freestream turbulence conditions, respectively. The freestream turbulence intensity levels were 1.0% and 3.9% by the

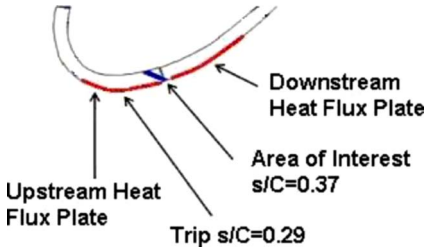


**Fig. 2 Schematic of area of interest**

time the flow reached $s/C=0.37$ on the vane suction side. The vane was constructed of low conductivity polyurethane foam with thermal conductivity $k=0.048$ W/m K. The area studied was between $s/C=0.37$ and $s/C=0.57$ on the suction side of the vane. A detailed schematic of the region of interest is shown in Fig. 2. Rows of dimples or film cooling holes were located between $s/C=0.35$ and $s/C=0.37$. For tests conducted with an upstream trip, a 0.4 mm diameter tripwire was placed at $s/C=0.28$. A uniform heat flux was applied using electrical heating of the stainless steel foils attached to the vane in the region of interest as well as upstream of the region of interest (upstream heating took place over the range $0.16<s/C<0.35$).

The pressure coefficient distribution around the vane was measured in previous studies [9,10], and is shown in Fig. 3. Note that the region over which these tests were conducted was immediately downstream of a strong favorable pressure gradient.

Figure 4 is a schematic of the dimple geometries for the elliptical, teardrop, and diffuser shaped dimples tested in the study as well as the shaped film cooling hole tested. For the three dimple geometries, the pitch was $2d$. The shaped film cooling holes had a pitch of $1.1d$. For all geometries tested, $d$ was the maximum spanwise width of the hole or dimple. This was about 10 mm for all geometries tested.

For the heat transfer measurements, a 50 $\mu$m thick stainless steel heat flux foil was used to apply a uniform heat flux on the surface of the vane. The surface temperature distribution, $T_w$, between $s/C=0.37$ and $s/C=0.55$ was measured using a FLIR ThermaCAM P20 infrared camera. The camera was calibrated in situ using two type E thin ribbon thermocouples located at the rear of the test area. These thermocouples were covered with a thin layer of tape and the entire test area was painted flat black to ensure a uniform emissivity over the entire test surface.

The convective heat transfer coefficient was determined through the following equation:

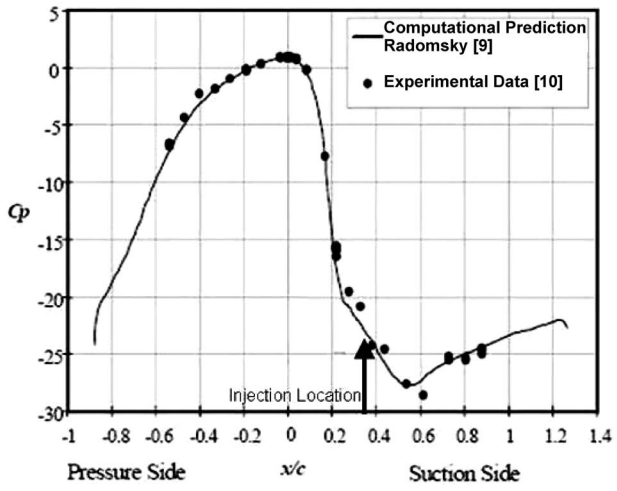


**Fig. 3 $C_p$ distribution for the vane**

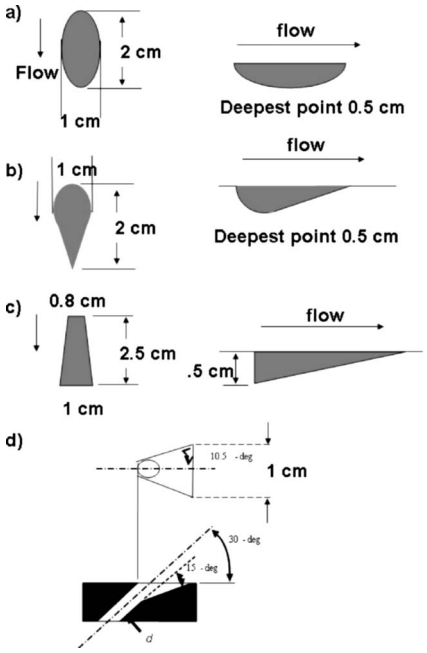


**Fig. 4 Schematic of (*a*) elliptical dimple, (*b*) teardrop dimple, (*c*) diffuser dimple, and (*d*) shaped film cooling hole**

$$h = \frac{q_{\text{electrical}} - q_{\text{radiation}} - q_{\text{conduction}}}{T_w - T_\infty} \tag{2}$$

where $q_{\text{radiation}}$ and $q_{\text{conduction}}$ were the heat fluxes lost due to radiation from the surface and conduction through the foam substrate. The mainstream temperature, $T_\infty$, was measured using a type E thermocouple near the leading edge of the vane. The conduction correction and radiation correction were calculated using Eqs. (2) and (3) as follows:

$$q_{\text{conduction}} = \frac{-k}{l}(T_w - T_i) \tag{3}$$

$$q_{\text{radiation}} = \varepsilon\sigma(T_w^4 - T_\infty^4) \tag{4}$$

$T_i$ was measured by attaching a surface thermocouple to the inside surface of the test vane. The magnitudes of the conduction and radiation heat fluxes were each about 5% of total heat flux.

The bias uncertainty in the temperature measurements was estimated to be less than 1 K. The overall uncertainty in the heat transfer coefficient was established by repeating data points at a given condition during the same test and by repeating tests on different days. The precision uncertainty was found to be ±3%. This caused an uncertainty of 2–5 $\text{W/m}^2\,\text{K}$, depending on the case. These uncertainties lead to an uncertainty of about ±5% in $h/h_0$ values.

## 3 Results

**3.1 Boundary Layer Measurements.** In order to quantify the state of the boundary layer approaching the row of film cooling holes or dimples, the boundary layer profiles for the case of a tripped and an untripped approach condition were measured immediately upstream of the $s/C=0.35$ position. This is $0.07C$ downstream of the 0.4 mm tripwire. The boundary layer profiles for the tripped and untripped cases are shown in Fig. 5, along with correlations for laminar and turbulent profiles. As can be seen in Fig. 5, the case for the tripped approach flow had a profile that very closely matched the 1/7 power law turbulent profile. Establishing that the trip was fully effective in tripping the boundary layer was an important factor in this study. We did this by testing

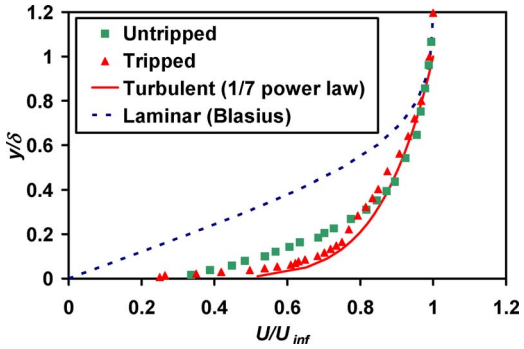


**Fig. 5 Boundary layer profiles at $s/C=0.35$ for tripped and untripped approach conditions**

two larger trips (0.8 mm and 1.7 mm) at the same location. The two larger trips were found to have the same effect on heat transfer augmentation as the 0.4 mm trip wire. This indicates that the trip wire was fully effective in tripping the approach boundary layer at the measurement location. For the untripped approach condition, the boundary layer profile falls between the laminar and turbulent profiles, suggesting a transitional boundary layer. The boundary layer thicknesses with and without the trip were found to be $\delta=3.2$ mm and 1.2 mm, respectively. The shape factors for the tripped and untripped boundary layers are $H=1.28$ and $H=1.64$, respectively. The shape factor for the untripped case was significantly larger than would be expected for a turbulent boundary layer but much lower than what would be expected of a laminar boundary layer, indicating a transitional boundary layer. The shape factor for the tripped boundary layer was consistent with the expected value for a fully turbulent case.

**3.2 Effect of Shaped Holes With Blowing.** The heat transfer coefficient downstream of a row of active fan shaped film cooling holes was measured. The geometry of the fan shaped film cooling holes can be seen in Fig. 4. The film cooling holes were tested at $\text{Re}=1.06\times10^6$ and high mainstream turbulence intensity conditions for both a tripped and an untripped approach flow and a heated and unheated starting length. Figure 6 shows the laterally averaged heat transfer coefficient augmentation due to the fan shaped film holes at several blowing ratios for an untripped approach flow with a heated starting length. Also plotted are the heat transfer augmentations due to a row of cylindrical cooling holes from Harrison et al. [11]. The laterally averaged $h$ values shown in Fig. 6 are all normalized to the smooth, untripped, low freestream turbulence baseline. Besides a very small region immediately downstream of the film cooling holes ($0.37<s/C<0.39$), the heat

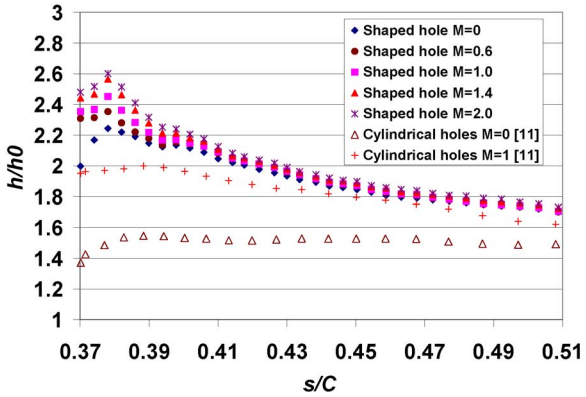


**Fig. 6 $h/h_0$ due to shaped hole film cooling: $\text{Re}=1.06\times10^6$, high *Tu*, untripped approach flow, HSL, untripped reference condition**

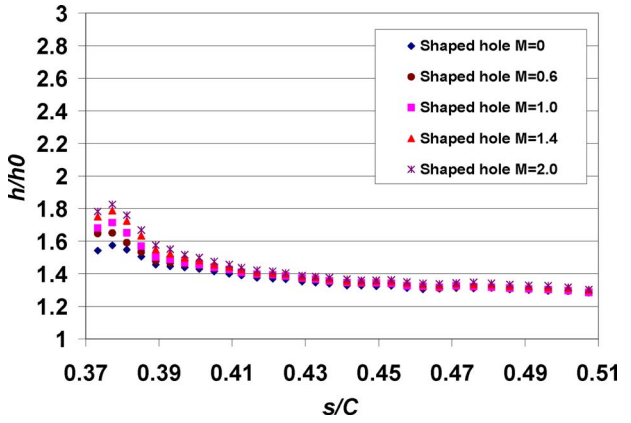


**Fig. 7** $h/h_0$ **due to shaped hole film cooling: Re=1.06×10⁶, high *Tu*, untripped approach flow, HSL, tripped reference condition**

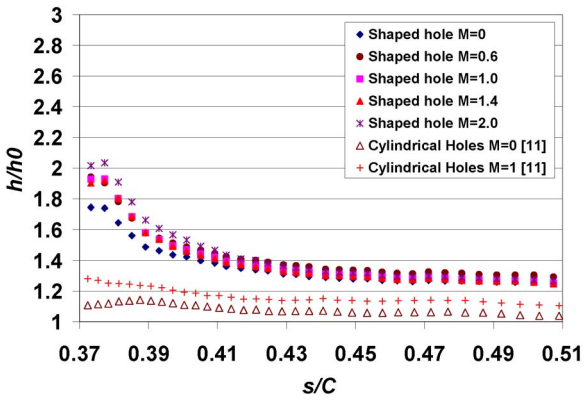


**Fig. 8** $h/h_0$ **due to shaped hole film cooling: Re=1.06×10⁶, high *Tu*, tripped approach flow, HSL, tripped reference condition**

transfer augmentation behind the shaped film cooling holes was found to be independent of blowing ratio or the presence of blowing at all. The nonblowing $M=0$ case had the same heat transfer augmentation as all the blowing ratios tested for $s/C>0.39$. This suggests that over the majority of the domain, the main cause of the increase in heat transfer is the geometry of the film hole and not the presence of blowing. The general trend showed $h/h_0$ values greater than 2.2 immediately downstream of the holes. The overall heat transfer augmentation of the shaped film cooling holes was very similar to the cylindrical film holes with $M=1.0$. In contrast to the shaped holes, blowing from the cylindrical holes had a significant effect. Blowing at $M=1.0$ from cylindrical holes caused as much as a 25% increase in $h/h_0$.

If the same heat transfer data shown in Fig. 6 are normalized to the smooth tripped baseline condition, the relative heat transfer augmentations are much lower. These data are shown in Fig. 7. After peak values of $h/h_0=1.4-1.8$ immediately downstream of the film holes, the augmentation levels quickly decreased to a level of about $h/h_0=1.3$. By normalizing to the smooth tripped baseline, the film cooling holes were seen to cause an additional heat transfer augmentation above and beyond transitioning the boundary layer to turbulence. The differences in heat transfer augmentation seen in Figs. 6 and 7 highlight the importance of taking into account varying reference conditions. In the following figures, a consistent reference condition was used in order to avoid confusion caused by varying reference conditions. The tripped high freestream turbulence conditions were chosen because they are most representative of actual engine operating conditions. With the exception of Fig. 6, all $h/h_0$ values presented in the study were normalized to the high *Tu*, tripped, smooth baseline at the appropriate Reynolds number and heated starting length condition.

When an upstream trip was used in addition to the film cooling holes, there was very little difference in downstream heat transfer augmentation when compared with film cooling holes with no upstream trip. Figure 8 shows laterally averaged heat transfer augmentation downstream of the shaped film cooling holes with an upstream trip. The only difference seen between the upstream trip and no upstream trip heat transfer augmentation are slightly higher peak levels immediately downstream of injection for the case with an upstream trip. Also shown in Fig. 8 are the cylindrical hole heat transfer augmentation levels from Ref. [11]. The shaped holes were seen to have about a 20% increase in $h_f/h_0$ relative to the cylindrical holes. This shows that for the heated starting length case, there is an effect of hole shape on the heat transfer augmentation.

The heat transfer augmentation downstream of the fan shaped film cooling holes was also measured for the case of no upstream heating. Using a configuration with no upstream heating is useful because it allows for the hydrodynamic effects of the flow to be isolated, since there is no upstream thermal boundary layer. The upstream heating case is useful because it more realistically models a real turbine airfoil, where the whole surface is heated. The heat transfer augmentation for the shaped film cooling holes with no upstream heating with an untripped and a tripped boundary layer are shown in Figs. 9 and 10, respectively. For both the tripped and untripped approach conditions, the peak seen directly downstream of the film holes was reduced when compared with the cases with upstream heating. The large peak just downstream of injection seen in the upstream heating case is presumably attributable to the formation of a new thermal boundary layer. The smaller peak heat transfer augmentation seen in Figs. 9 and 10 are solely attributable to the hydrodynamic effects of the film holes on the boundary layer, since there is no thermal boundary layer history at this point. Heat transfer augmentation levels for the case of a tripped approach boundary layer were slightly higher than those for the untripped approach boundary layer throughout the domain. As seen in Fig. 10, the shaped holes with a tripped approach boundary layer had slightly higher heat transfer augmentation levels than the cylindrical film cooling holes for the same condition, again suggesting an effect of hole shape on the heat transfer coefficient. For both the tripped and untripped approach boundary layers, the heat transfer augmentation downstream of the shaped film cooling holes was independent of blowing, suggesting that the hole geometry is a more important factor than blowing from the hole. The shaped hole heat transfer augmentation of Dittmar et

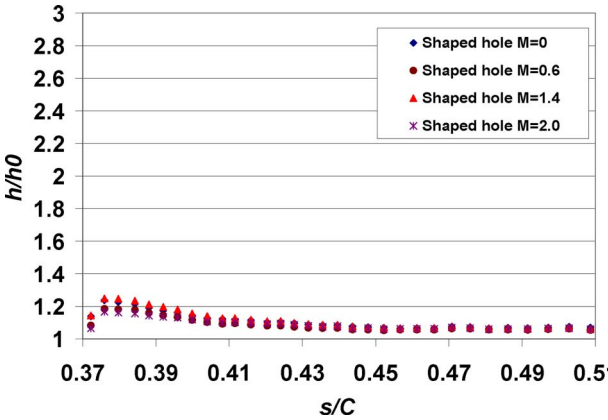


**Fig. 9** $h/h_0$ **due to shaped hole film cooling: Re=1.06×10⁶, high *Tu*, untripped approach flow, UHSL, tripped reference condition**

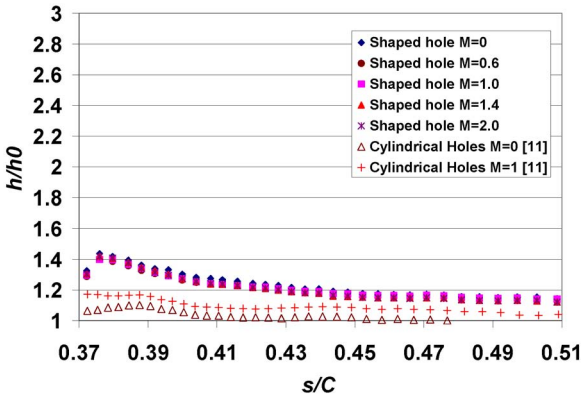


**Fig. 10** $h/h_0$ **due to shaped hole film cooling: Re=1.06×10^6, high *Tu*, tripped approach flow, UHSL, tripped reference condition**

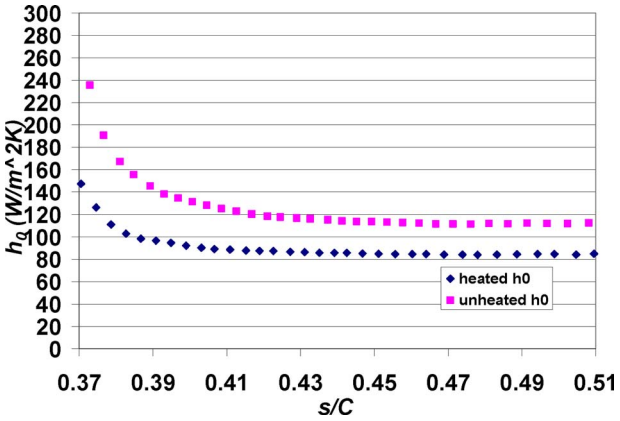


**Fig. 12** $h_0$ **values for heated and unheated starting length, tripped approach condition**

al. [7] has peak values immediately downstream of injection that range $h/h_0=1.4-1.6$ for a similar shaped hole configuration, decreasing to near unity with increasing downstream distance for the case of an unheated starting length. The data of Dittmar et al. [7] does show some blowing ratio dependence immediately downstream of injection. Figure 11 shows the HSL and UHSL data for both shaped holes and cylindrical holes for a nonblowing and $M=1$ case. This figure highlights that the upstream heating condition had a much larger effect on the shaped film cooling holes when compared with the cylindrical cooling holes. This greater effect for the shaped holes may be attributed to the wider coverage for the shaped holes.

Figure 12 shows the baseline heat transfer coefficient levels for the heated and unheated starting length cases with a tripped approach condition and low freestream turbulence. The smooth $h_0$ condition for the no upstream heating case was found to be about 30% higher than the $h_0$ with upstream heating. The unheated starting length effect should disappear after a certain downstream distance, causing the unheated and heated starting length cases to collapse. Using a standard correlation, the distance required for the two curves to merge to within 5% of each other is significantly longer than the extent of the region examined. The difference in reference conditions for the heated and unheated starting lengths provides insight into the differences in the downstream $h/h_0$ values seen in Figs. 6–11. Dimensional heat transfer coefficient values downstream of the shaped film cooling holes were nominally the same regardless of the upstream heating condition or state of the approach boundary layer. The differences seen in $h/h_0$ are primarily due to the 30% increase in the $h_0$ reference condition for the unheated starting length case.

**3.3 Effect of Hole Shape With No Blowing.** Convective heat transfer coefficients behind rows of elliptical, teardrop, and diffuser shaped indentions were measured between $0.37<s/C<0.51$. These dimples were meant to approximate various film cooling hole geometries. Since the shaped film cooling holes tested above caused the same heat transfer augmentation regardless of whether the holes were active or not, the heat transfer augmentation downstream of the various dimple shapes was assumed to be representative of what an actual active film cooling hole of each shape would be. This hypothesis was only tested for the case of shaped film cooling holes. Cylindrical hole data from Ref. [11] shown in Fig. 6 suggests that this assumption is not very good for an untripped heated starting length approach condition; however, for the tripped HSL approach condition shown in Fig. 8, this assumption is reasonable. For each test surface, the mainstream Reynolds number, mainstream turbulence intensity, and approach boundary layer condition were varied giving a total of 8 different configurations for each surface. Figure 13 shows the values of $h$ for all configurations at a streamwise position of $s/C=0.41$. For an untripped approach condition, all dimple shapes significantly increased the heat transfer coefficient relative to the smooth untripped baseline case. For a tripped approach condition, the heat transfer coefficient was augmented for the dimpled surfaces relative to the smooth tripped case, but at a much lower level. The relatively small change in $h$ for the various dimple

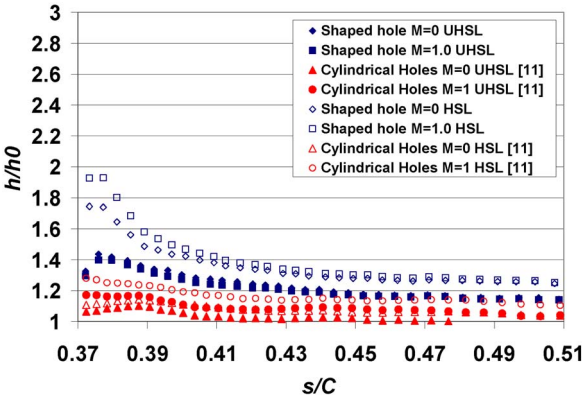


**Fig. 11 Effect of HSL and UHSL on $h/h_0$: Re=1.06×10^6, high *Tu*, untripped approach flow, tripped reference condition**

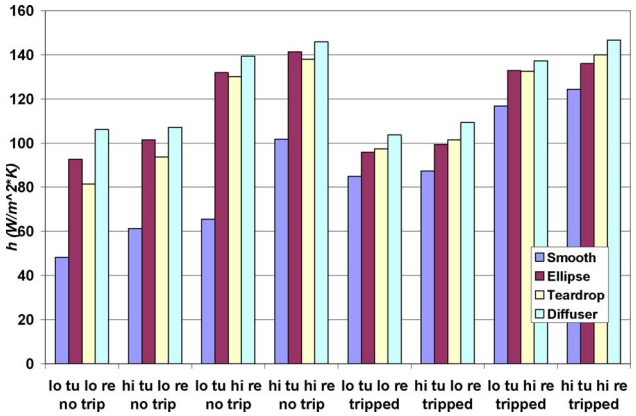


**Fig. 13 Laterally averaged *h* values at *s/C*=0.41, all configurations**

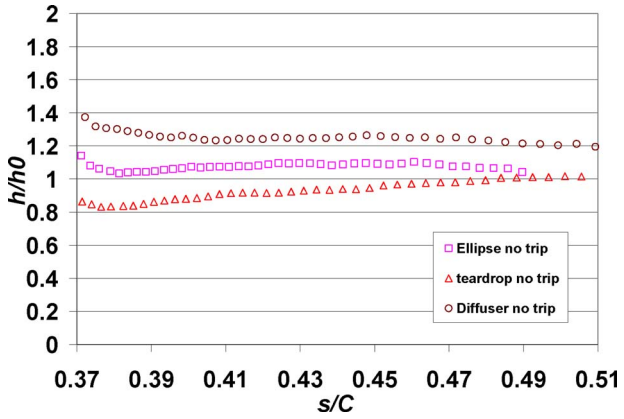


**Fig. 14 Effect of dimple shape on $h/h_0$; untripped approach condition, low *Tu*, Re=1.06×10^6, HSL tripped, high *Tu*, low Re reference**

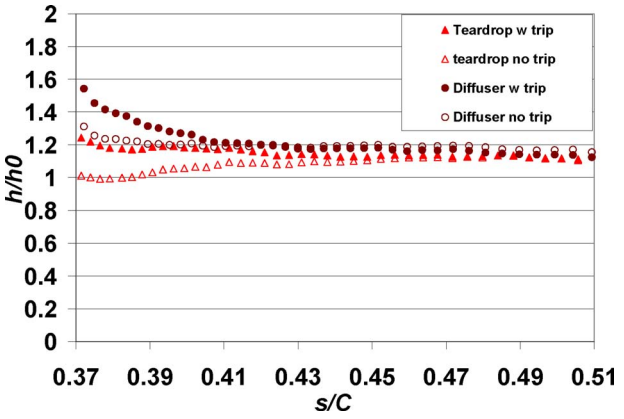


**Fig. 16 Effect of dimple shape on $h/h_0$; tripped and untripped approach conditions, low *Tu*, Re=1.88×10^6, HSL tripped, high *Tu*, high Re reference**

configurations when comparing tripped and untripped upstream flows suggests that the primary effect of dimples is to induce transition to turbulent boundary layer flow.

The different dimple shapes caused different levels of heat transfer augmentation relative to the smooth tripped baseline. This reference condition is used for Figs. 14–17 because it is believed to be the most representative reference for engine operating conditions. As seen in Fig. 14, for the untripped condition the diffuser dimples caused the highest increase in $h$ and the teardrop dimples caused the lowest increase with elliptical dimples falling in the middle. The increase caused by the diffuser dimples is roughly 30% higher than the increase caused by the teardrop dimples. In fact, the teardrop dimples had $h/h_0$ values less than unity for $s/C=0.37-0.49$, indicating that the teardrop dimples were not as effective in tripping the boundary layer as the trip wire. This suggests that certain film cooling hole geometries are more effective in tripping the boundary layer.

Figure 15 shows the effect of the various dimple shapes on the heat transfer coefficient for both the tripped and untripped approach conditions for $\mathrm{Re}=1.06\times10^6$ and low freestream turbulence. The elliptical geometry data are available but are not included in this figure, as well as Figs. 15–17, for clarity. The elliptical dimples were chosen for omission because when there was variation in $h/h_0$ due to dimple shape, the elliptical dimples were always bracketed by the shaped and teardrop dimples. Tripping the approach flow has the smallest effect on the heat transfer coefficient behind the diffuser dimples. This suggests that the diffuser dimples alone were fully effective in tripping the boundary layer. The upstream trip had the largest effect on the heat transfer coefficient behind the teardrop dimples, causing a 33% increase in the heat transfer augmentation relative to the untripped case. This suggests that the teardrop dimples alone were not a fully effective boundary layer trip. For the diffuser dimples at both trip conditions and the teardrop dimples with a tripped approach boundary layer, an increase of about 20% beyond the smooth tripped baseline condition was seen. This suggests that the diffuser dimples are providing extra heat transfer augmentation beyond causing fully turbulent boundary layer flow.

The effect of the various dimple shapes on the heat transfer augmentation for both the tripped and untripped approach conditions for the higher Reynolds number of $\mathrm{Re}=1.88\times10^6$ and the low freestream turbulence condition is shown in Fig. 16. In this case, the reference $h_0$ case was the smooth, tripped, high turbulence, $\mathrm{Re}=1.88\times10^6$ condition. In contrast to the lower Reynolds number case, there was a much smaller shape effect on the heat transfer coefficient. This suggests that at this higher Reynolds number, the boundary layer is more easily tripped to turbulence and the precise shape of a film cooling hole is not an important factor. The addition of an upstream trip caused a slight increase in the heat transfer augmentation for all the shapes between $0.37<s/C<0.43$, but there was no difference in the tripped and untripped cases for $s/C>0.43$.

The effect of varying the freestream turbulence intensity for the low Reynolds number case with no upstream trip is shown in Fig. 17. For the low Reynolds number, elevated freestream turbulence

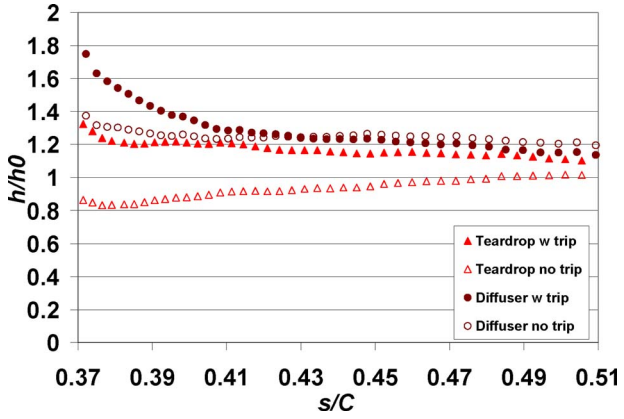


**Fig. 15 Effect of dimple shape $h/h_0$; tripped and untripped approach conditions, low *Tu*, Re=1.06×10^6, HSL tripped, high *Tu*, low Re reference**

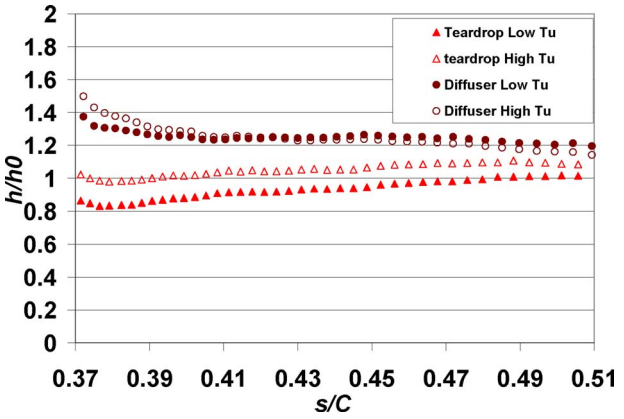


**Fig. 17 Effect of varying freestream turbulence intensity on $h/h_0$, no trip, Re=1.06×10^6, HSL**

caused an increase of about 20% in heat transfer augmentation for the teardrop shaped depression. The diffuser dimples had no increase in $h/h_0$ due to the higher turbulence intensity, presumably due to the diffuser dimples causing a more complete transition to turbulence than the other shapes. For the other conditions tested, including high Reynolds number and tripped approach boundary layers, the elevated turbulence level had no effect on the heat transfer coefficient.

## 4 Conclusions

Heat transfer measurements were conducted on the suction side of a scaled up gas turbine vane behind rows of shaped film cooling holes and various dimple geometries designed to simulate different film cooling hole shapes. For the heat transfer coefficient behind the row of shaped film cooling holes, unheated and heated starting length conditions were tested for the case of high mainstream turbulence and $\mathrm{Re}=1.06\times10^6$. For both the heated and unheated starting lengths, the heat transfer augmentation downstream of the shaped film cooling hole was independent of blowing ratio. When using film cooling from shaped holes, the heat transfer coefficient augmentation was much greater when using upstream heating compared with that for an unheated started length, particularly near the hole. This greater augmentation of heat transfer coefficient when using a heated starting length can be attributed to the displacement of the thermal boundary layer by the injected gas. Considering that many studies of the effects of film cooling injection on heat transfer enhancement employ an unheated starting length, the large effect of the upstream heating is a significant finding, particularly since the upstream heating is a more realistic condition.

Contrasting results for shaped and cylindrical holes were seen. With upstream heating, the shaped holes caused a much greater enhancement of heat transfer than that for cylindrical holes. These results suggest that blowing from shaped holes displaces the thermal boundary layer more effectively than blowing from cylindrical holes. When an unheated starting length was used, the difference in heat transfer enhancement for shaped and cylindrical holes was less.

Additionally, the heat transfer coefficient was measured downstream of rows of elliptical, teardrop, and diffuser shaped dimples. For a case with an untripped approach boundary layer, all of the dimple geometries caused downstream $h/h_0$ values between 0.8 and 1.4 relative to the smooth tripped reference. This leads to the conclusion that the primary effect of the dimples was to promote transition, but that different shapes were more or less effective in causing transition to turbulence. The diffuser dimples caused the largest augmentation and the teardrop dimples caused the lowest augmentation. The $h/h_0$ values that were greater than 1.0 further imply that the dimples not only caused transition to turbulence but had an additional effect on the boundary layer that increased the heat transfer coefficient beyond that of a turbulent boundary layer. Increasing the overall Reynolds number of the flow did not significantly change the heat transfer augmentation levels relative to the smooth tripped baseline at the appropriate Reynolds number. One effect seen at the higher Reynolds number was a decreased sensitivity of $h/h_0$ on dimple shape, suggesting that at the higher Reynolds number the boundary layer was more easily caused to be fully turbulent.

All of the augmentation factors presented in this paper were normalized to the smooth tripped baseline case. The augmentation factors were modest, usually showing a 10–20% increase in heat transfer coefficient downstream of a row of holes or dimples. This modest augmentation was a function of the baseline condition used. Had the smooth untripped baseline condition been used to normalize the data, a much stronger heat transfer augmentation of around two times the baseline would have been seen. The smooth untripped baseline was believed to be a laminar/transitional boundary layer, and the addition of a row of cooling holes caused the boundary layer to become turbulent, which caused large increases in the heat transfer coefficient. This shows the importance of correctly determining the flow conditions that exist on an airfoil without film cooling when evaluating the impact of film cooling. Clearly if the presence of coolant holes promotes early transition, the large increase in heat transfer coefficient may be quite detrimental.


## Acknowledgment

The authors gratefully acknowledge the support of GE Energy in the completion of this research.


## Nomenclature

$C$ = vane chord length
$C_p$ = pressure coefficient
$d$ = dimple diameter or film cooling hole diameter
$h$ = heat transfer coefficient
$H$ = Clauser shape factor
$k$ = thermal conductivity
$K$ = acceleration parameter, $(\nu/U_e^2)(dU_e/dx)$
$l$ = thickness of vane wall
$M$ = film cooling blowing ratio
$q''$ = heat flux
$p$ = spacing between dimples
$s$ = streamwise surface distance from stagnation
$T$ = temperature
$U$ = flow velocity

### Greek

$\sigma$ = Stephan–Boltzmann constant

### Subscripts

$e$ = edge
$i$ = inner vane surface
$0$ = smooth baseline reference
$w$ = vane wall or surface
$\infty$ = freestream

## References


[1] Eriksen, V. L., and Goldstein, R. J., 1974, "Heat Transfer and Film Cooling Following Injection Through Inclined Circular Tubes," ASME J. Heat Transfer, **96**, pp. 239–245.
[2] Hay, N., Lampard, D., and Saluja, C. L., 1985, "Effects of Cooling Films on the Heat Transfer Coefficient on a Flat Plate With Zero Mainstream Pressure Gradient," ASME J. Eng. Gas Turbines Power, **107**, pp. 105–110.
[3] Ammari, H. D., Hay, N., and Lampard, D., 1990, "The Effect of Density Ratio on the Heat Transfer Coefficient for a Film Cooled Flat Plate," ASME J. Turbomach., **112**, pp. 444–450.
[4] Liess, C., 1975, "Experimental Investigation of Film Cooling With Ejection From a Row of Holes for the Application to Gas Turbine Blades," ASME J. Eng. Power, **97**, pp. 21–27.
[5] Sargison, J. E., Guo, S. E., Oldfield, M. L. G., Lock, G. D., and Rawlinson, A. J., 2002, "A Converging Slot-Hole Film Cooling Geometry—Part 1: Low-Speed Flat-Plate Heat Transfer and Loss," ASME J. Turbomach., **124**, pp. 453–460.
[6] Lu, Y., Dunghel, A., Ekkad, S. V., and Bunker, R., 2007, "Effect of Trench Width and Depth on Film Cooling From Cylindrical Holes Embedded in Trenches," ASME Paper No. GT2007-27388.
[7] Dittmar, J., Shulz, A., and Wittig, S., 2003, "Assessment of Various Film-Cooling Configurations Including Shaped and Compound Angle Holes Based on Large-Scale Experiments," ASME J. Turbomach., **125**, pp. 57–64.
[8] Rutledge, J. L., Robertson, D. R., and Bogard, D. G., 2005, "Degradation of Film Cooling Performance on a Turbine Vane Suction Side Due to Surface Roughness," ASME Paper No. GT2005-69045.
[9] Cutbirth, M. J., 2000, "Turbulence and Three Dimensional Effects on a Film Cooled Turbine Vane," Ph.D. thesis, University of Texas, Austin, TX.
[10] Radomsky, R. W., 2000, "High Freestream Turbulence Studies on a Scaled-Up Stator Vane," Ph.D. thesis, University of Wisconsin-Madison, Madison, WI.
[11] Harrison, K. L., Dorrington, J. R., Dees, J. E., Bogard, D. G., and Bunker, R. S., 2007, "Turbine Airfoil Net Heat Flux Reduction With Cylindrical Holes Embedded in a Transverse Trench," ASME Paper No. GT2007-27996.